Mechanical characterisation of human and porcine scalp tissue at dynamic strain rates

Antonia Trotta[1], Aisling Ní Annaidh[1, 2]

[1] School of Mechanical & Materials Engineering, University College Dublin, Belfield, Dublin 4, Ireland

[2] UCD Charles Institute of Dermatology, School of Medicine and Medical Science, University College Dublin, Belfield, Dublin 4, Ireland

Abstract

Several biomedical applications require knowledge of the behaviour of the scalp, including skin grafting, skin expansion and head impact biomechanics. Scalp tissue exhibits a non-linear stress-strain relationship, anisotropy and its mechanical properties depend on strain rate. When modelling the behaviour of the scalp, all these factors should be considered in order to perform realistic simulations. Here, tensile tests at strain rates between 0.005 – 100 s^{-1} have been conducted on porcine and human scalp in order to investigate the non-linearity, anisotropy, and strain rate dependence of the scalp mechanical properties. The effect of the orientation of the sample with respect to the Skin Tension Lines (STLs) was considered during the test. The results showed that anisotropy is evident in the hyperelastic response at low strain rates (0.005 s^{-1}) but not at higher strain rates (15-100 s^{-1}). The mechanical properties of porcine scalp differ from human scalp. In particular, the elastic modulus and the Ultimate Tensile Strength (UTS) of the porcine scalp were found to be almost twice the values of the human scalp, whereas the stretch at failure was not found to be significantly different. An anisotropic hyperelastic model (Gasser-Ogden-Holzapfel) was used to model the quasi-static behaviour of the tissue, whereas three different isotropic hyperelastic models (Fung, Gent and Ogden) were used to model the behaviour of scalp tissue at higher strain rates. The experimental results outlined here have important implications for those wishing to model the mechanical behaviour of scalp tissue both under quasi-static and dynamic loading conditions.

Keywords: scalp, mechanical characterization, skin, head impact

1. Introduction

The scalp is the most external part of the head; it is a multi-layered tissue made up of five principal layers: skin, connective tissue, aponeurosis, loose areolar tissue and periosteum. The first three layers of the scalp are held together forming a single unit which is often referred to as scalp and can be easily detached from the skull [1]. The skin is the outer layer of the scalp. It has a similar structure to skin from other parts of the body except that hair is present in large amounts. However, Kumar et al. [2] showed that the skin layer contained about 30% of collagen with respect to its cross-sectional area and only 0.5% of elastin; a lower value of elastin compared with skin from the wrist or abdomen. The connective tissue contains collagen and elastin, adipose cells, arteries, veins and nerves supplying the scalp. The aponeurosis is made up of dense fibrous tissue and is the strongest layer of the scalp. It contains two layers of fascia which connect the two bellies of the occipitofrontalis muscle through an inelastic fascial membrane. The loose areolar tissue connects the aponeurosis to the periosteum and facilitates movements between the scalp and the skull. This is the area where large

***Corresponding Author**: A. Trotta (trottaa@ucd.ie)*

amount of blood is collected after trauma or surgery. The periosteum is the last layer of the scalp. It is attached to the skull by connective tissue fibres. The thickness of the scalp depends on age and location [3] and average values range between 3 mm in children and 8 mm in adults [4, 5]. The thickness of each constituent of the scalp depends on age and gender [6]. Hori et al. reported that for an adult male (30-50 years old) the skin (epidermis and dermis) accounts for 30.5% of the scalp, the connective tissue for 38.5%, and the aponeurosis and loose areolar tissue for 31%. Several biomedical applications require knowledge of the mechanical behaviour of the scalp, including skin grafting, skin expansion [7-9] and head impact biomechanics [10-15]. Indeed, the scalp was previously found to substantially affect head kinematics and impact energy during helmet testing [11, 16]. From a mechanical point of view, the scalp is a complex tissue; it exhibits a non-linear stress-strain relationship, anisotropy and its mechanical properties depend on strain rate. In order to accurately predict the behaviour of this tissue and to perform realistic numerical simulations, this mechanical behaviour requires in depth investigation.

In general, researchers have typically assumed that the scalp behaves as a linear elastic material, with properties obtained by the linearization of skin properties from other parts of the body [17-19]. Only a few works have studied scalp tissue specifically and its mechanical properties. Gambarotta et al. [20] performed in-vivo experimental testing on undermined skin flaps for the characterization of human scalp skin and showed that the scalp is highly non-linear with an initial soft behaviour followed by a much stiffer part. Galford and McElhaney [21], performed stress-relaxation and creep tests on monkey scalp and concluded that the scalp is a linear viscoelastic material. Jacquemound et al. [22] performed dynamic tensile tests on forehead skin showing that, at high speed, the ultimate stress (4.6 MPa) is similar to the value of quasi-static tests, but that the ultimate tensile strain is half of the value reported for quasi-static tests. Recently, Falland-Cheung et al. [23] performed tensile tests at 0.042 s^{-1} of strain rate on human scalp tissue with the aim of providing data for application in the impact biomechanics area. They tested specimens from different scalp locations: left temporal, fronto-parietal, right temporal and occipital. No significant differences were observed comparing the tensile strength between males and females. However, the gender was found to affect the elastic modulus of the occipital region and the elongation properties. The elastic modulus of the scalp in female donors decreased with age, whereas no correlation with age was found amongst male donors.

Constitutive models describe the mechanical behaviour of materials through mathematical models in which the parameters often have physical meaning. These models play a key role in the predictive capability of computational models. Scalp tissue exhibits a non-linear and anisotropic (at low strain rates) stress-strain relationship, which is typical of many soft tissues, due to its internal composition of fibres embedded within a gel-like ground substance. This complex behaviour can be described using different constitutive models, each of them suitable for specific applications.

In order to study the non-linear behaviour, a non-linear version of the classic elasticity theory was developed by researchers like Ogden, Fung and Rivlin [24-27]. Hyperelasticity, which is a particular case of non-linear elasticity, uses a strain energy function, W, to describe in energetic terms the mechanical behaviour of this class of material. Initially developed to describe the behaviour of polymeric materials [27], hyperelastic models are now commonly applied to biological soft tissues [25, 28-30]. Hyperelastic constitutive models have been developed for both isotropic and anisotropic materials. Examples of isotropic hyperelastic models are Neo-hookean, Gent, Fung, Mooney-Rivlin and Ogden. They have been used to describe skin, artery, brain, ligament and tendon [31-39]. Anisotropy was introduced in soft tissue modelling to incorporate the effect of the collagen fibres into

the constitutive relation. Lanir [40] was one of the first to include anisotropy, followed by a number of researchers: Holzapfel, Gasser and Ogden [30, 41].

In this study, non-linearity, anisotropy, and the strain rate dependence of scalp's mechanical properties have been investigated considering different factors: the orientation of the skin tension lines, the origin of the scalp (porcine vs human) and the strain rate. Results of the test on porcine scalp, which is commonly accepted as being the most suitable human skin surrogate [42], were compared with those of human cadaver scalp. Experimental data has been fit to different non-linear hyperelastic models and a statistical analysis has been performed to evaluate the effect of each factor.

2. Materials & Methods

2.1 Specimens preparation

2.1.1 Porcine scalp

Porcine heads were sourced from 22 weeks old, mixed gender pigs and were obtained from a local abattoir within 4-6 hours of slaughter. The scalp was excised from the porcine head using a scalpel and specimens were cut using a dogbone cutter (dimensions specified in Figure 1) in different orientations with respect to the skin tension lines (STLs). Specimens were stored for not more than 3 months in a freezer at -20°C and defrosted the day of the test. Specimens were kept in saline solution prior to testing to avoid dehydration of samples.

2.1.2 *Human scalp*

The ethics committee within KU Leuven approved the use of human cadaver heads for testing (Ethical approval n. NH0192017-02-02). Five Caucasian human heads were obtained from the KU Leuven Anatomy Centre (3 females and 2 males, age between 73-89). The heads were transported and stored in the test lab at 4°C. The heads were shaved, and the scalp was excised using a scalpel and stored in a freezer at -80°C. The dogbone cutter described in Figure 1 was used to cut the specimens. Specimens were stored in saline solution prior to testing to avoid dehydration of samples.

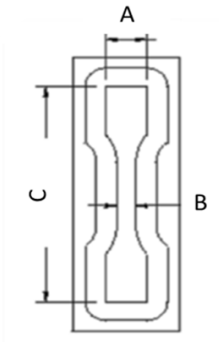

Harvested from	A [mm]	B [mm]	C [mm]
Porcine head	9.525	3.175	63.5
Human cadaver head	19.05	12.70	76.30

Figure 1: dog-bone sample dimensions.

2.2 Elastic wave propagation

In order to test the anisotropy of the scalp and to identify the orientation of the skin tension lines on the pig forehead, a Reviscometer® device was used [43]. The Reviscometer® RVM 600 device (Courage & Khazaka Electronic GmbH, Kln, Germany) is a commercial device which consists of two probes, an emitter and receiver, placed 2 mm apart (Figure 2). The emitter releases an acoustic shock-

wave by impacting the scalp with a force of 1 N and the receiver measures the time (Resonance Running Time (RRT)) for that wave to travel from the emitter to the receiver [44]. The device can take measurements every 10 degrees about a full 360 degrees. This test allows the researcher to determine, non-destructively and non-invasively, whether the tissue is anisotropic and identifies the orientation of the skin tension lines [43, 45-47]. The test was repeated three times on each sample and the average values were recorded. The orientation of the skin tension lines on the human scalp was, instead, identified based on the results reported by Langer [48].

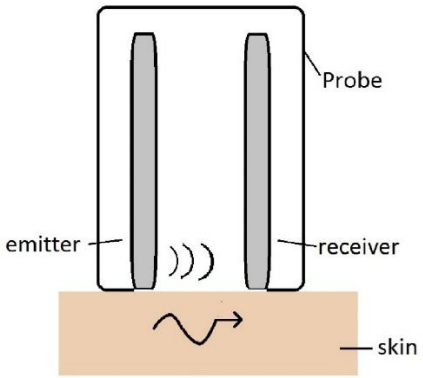

Figure 2: Basic schematic representing how the Reviscometer RVM 6oo works. The emitter releases an acoustic wave and the receiver measures the RRT (Resonance Running Time). The direction of lowest RRT indicates the orientation of skin tension lines. Reproduced from Deroy et al. [43].

2.2 Tensile tests

Quasi-static and dynamic tensile tests on porcine scalp were performed at University College Dublin, while dynamic tensile tests on human scalp were performed at Katholieke Universiteit Leuven. Tensile tests provide stress-strain relationships which are easy to quantify and model, since boundary conditions are well defined, and were, therefore, chosen to study the hyperelasticity of scalp tissue. Due to the anisotropy of the tissue, specimens were loaded parallel and perpendicular with respect to the STLs.

2.2.1 Quasi-static tensile test

After performing elastic wave propagation tests and having identified the orientation of the skin tension lines, porcine specimens were cut parallel and perpendicular to the orientation of the skin tension lines. Quasi-static tensile tests were conducted on porcine scalp samples in order to evaluate the non-linearity and to confirm anisotropy of the scalp. Tests were performed using a Hounsfield Universal Testing machine at room temperature (21±2°C). A 1 kN load cell was used to measure the force. Two reference dots were drawn on the extremities of the sample to measure the strain during the tests via video recording. A preload of 1 N was applied to the samples prior to testing in order to ensure that the specimens were strained from the beginning of the test. 24 specimens were tested in total, 12 parallel and 12 perpendicular with respect to the STLs. The width of the samples was 3.175 mm, the thickness was 2.92±0.20 mm and the gauge length was 35.03±3.36 mm. Perforated metal sheets were used to enhance grip on the samples. All tests were carried out at a strain rate of 0.005 s^{-1}. Results were analysed in terms of Cauchy stress and stretch.

2.2.2 Dynamic tensile tests

To quantify the effect of the strain rate, dynamic tensile tests were performed on porcine and human scalp. Based on the works of Perogamvros et al. [49] and Yoon et al. [50], a rig was developed to perform high strain rate tensile tests using the Rosand Zwick 5HV impact test machine (at University College Dublin) and an in-house built impact test machine (at Katholieke Universiteit Leuven). The main function of the rig was to convert the compressive loading of a drop tower machine into tensile loading of the specimens. Two main specifications were considered during the development of the system: 1) the symmetry of the device in order to avoid unpredictable loading conditions and 2) efficient grips in order to avoid slip of the specimens. The set up developed is shown in Figure 3. The device consists of two grips, one fixed and one moving. The upper grip is fixed to the load cell (Kistler 6 kN piezoelectric load cell), which is fixed to the rigid frame. The lower grip is fixed to a bar free to move in the vertical direction. When the impactor of the drop machine strikes the metal bar, the specimen is subjected to tensile loading. In order to minimise slippage of the specimen, sandpaper was used on the inner surfaces of the grips. The mass of the movable frame is 197 g, a value that determines the preload of the sample (1.93N). Tests were performed at three different strain rates, 15, 50 and 100 s^{-1} and at room temperature (21±2°C). A sampling rate of 200 kHz was used for the force readings. A square shape was drawn on the specimen and a high-speed camera (4000 frames per second and 1024x1024 resolution) was used to record each test and to determine the strain undergone by the specimen during the test using tracking software (Tracker video analysis and modelling tool). A laser system measured the starting point of the test and triggered the high-speed camera. A total of 72 porcine specimens were tested; 24 specimens for each level of strain rate (12 parallel and 12 perpendicular to the STLs). Whereas, 24 human specimens were tested; 8 for each level of strain rate (4 parallel and 4 perpendicular to the STLs). A Savitzky-Golay filter (order 1, framelen 21) was used to filter the data in Matlab (R2018a). Results were analysed in terms of Cauchy stress and stretch. A multiway ANOVA followed by a post-hoc test was used to compare the values of the elastic modulus, the ultimate tensile strength (UTS) and stretch at failure at different strain rates and orientations.

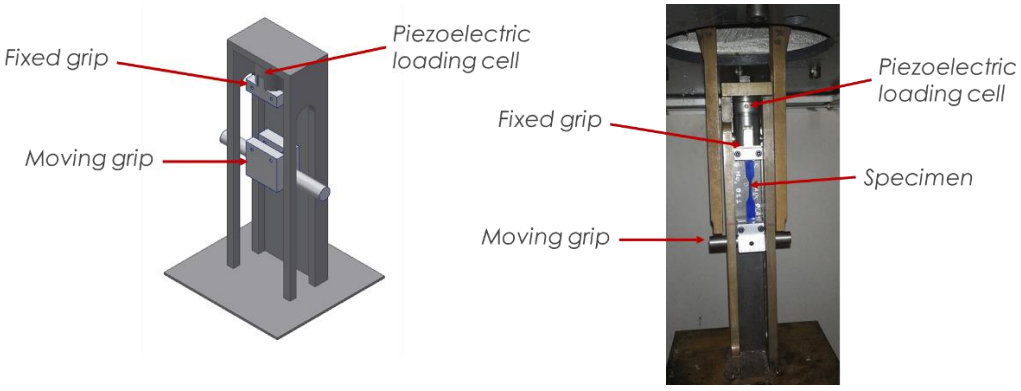

Figure 3: Customised experimental rig which converts the compressive loading of a drop tower machine into dynamic tensile loading. CAD model on the left and actual device on the right.

2.3 Data analysis & Fitting

Due to the anisotropy at low strain rates, quasi-static experimental data was fitted to the GOH hyperelastic model, following the procedure described by Ní Annaidh et al. [45] for incompressible materials. With this simplification, the equations necessary to describe the scalp behaviour are:

$$\sigma_{11} = \mu(\lambda_1^2 - \lambda_1^{-2}\lambda_2^{-2}) + 4\mu k_1 \alpha e^{k_2\alpha^2}[\kappa(\lambda_1^2 - \lambda_1^{-2}\lambda_2^{-2}) + (1-3\kappa)(\lambda_1^2\cos^2\gamma)] \quad \text{Eq. 1}$$

$$0 = \lambda_2^2 - \lambda_1^{-2}\lambda_2^{-2} + 4k_1 \alpha e^{k_2\alpha^2}[\kappa(\lambda_2^2 - \lambda_1^{-2}\lambda_2^{-2}) + (1-3\kappa)(\lambda_2^2\sin^2\gamma)] \quad \text{Eq. 2}$$

$$\alpha = \kappa(\lambda_1^2 + \lambda_2^2 - \lambda_1^{-2}\lambda_2^{-2}) + (1-3\kappa)(\lambda_1^2\cos^2\gamma + \lambda_2^2\sin^2\gamma) - 1 \quad \text{Eq. 3}$$

Where μ, k_1 and k_2 are material constants, λ_1 and λ_2 are the stretch in the direction of tension and in the lateral direction respectively, κ is the fibre dispersion, and γ is the angle between the fibres and the tensile direction (assumed equal to 41° from [45]). Since non-linear optimization procedures are often sensitive to the initial guess provided by the user [51], the initial guess for k_1 was found by calculating the slope of the non-linear part of the stress-stretch curve. k_1 is, indeed, related to the stiffening phase of the tensile tests and, therefore, the initial guess has a physical meaning [45]. In addition, k_1 and k_2 were varied over the same range proposed by Ní Annaidh et al. [45] (0-$1e^6$ for k_1 and 0-$1e^3$ for k_2) to check that the optimization procedure was not sensitive to the initial guess. The inputs of the curve fitting are σ_{11} and λ_1. λ_2, along with k_1, k_2, κ and μ are obtained during the optimization of Eq. 1 and Eq. 2. The initial guess for λ_2 was set to $\lambda_1^{-1/2}$ (assuming an isotropic incompressible material).

At high strain rates anisotropy is not evident and therefore, dynamic tensile data was fit to three different isotropic hyperelastic models: Fung (Eq 4) [52], Gent (Eq 5) [27] and Ogden (Eq 6) [53]. These three models are widely used to describe soft tissue behaviour and use strain energy functions to describe the material behaviour. Assuming incompressibility and in the case of uniaxial tension, these models can be easily written in terms of the stress-stretch relationships.

$$Fung: \quad \sigma_{11} = \frac{\mu}{\lambda} e^{\frac{b(\lambda+2)(\lambda-1)^2}{\lambda}}(\lambda^3 - 1) \quad \text{Eq. 4}$$

$$Gent: \quad \sigma_{11} = \frac{\mu J_m(\lambda^3-1)}{J_m\lambda + 3\lambda - \lambda^3 - 2} \quad \text{Eq. 5}$$

$$Ogden: \quad \sigma_{11} = \sum_n \mu_n(\lambda^{\alpha_n} - \lambda^{-\frac{1}{2}\alpha_n}) \quad \text{Eq. 6}$$

where μ is the initial shear modulus and b, J_m and α_i are parameters related to the stiffening effect. The fitting was conducted using MATLAB (R2018a). For the anisotropic model the experimental data was fit to the model using fminunc to run an optimization routine in MATLAB. For the isotropic fitting, the fitting tool available in MATLAB was used. For each parameter, the average estimated parameter in each group and the standard deviation were calculated, as well as the coefficient of determination (R^2) to evaluate the quality of the fit.

3. Results

3.1 Elastic wave propagation tests

Figure 4 (left) shows average values of RRT on the porcine scalp. This graph shows that the time taken for the wave to travel from the emitter to the receiver is different around a circular pattern on the porcine scalp and, therefore, that the porcine scalp is anisotropic. Knowing the distance between the two probes (2 mm), the speed of the wave can be calculated. Analysing the different times/speeds, the identification of the orientation of the skin tension lines is possible, since the wave propagates faster in the direction of skin tension lines [43]. Tests performed on porcine scalp showed that the orientation of the STLs across the forehead is horizontal (Figure 4 right).

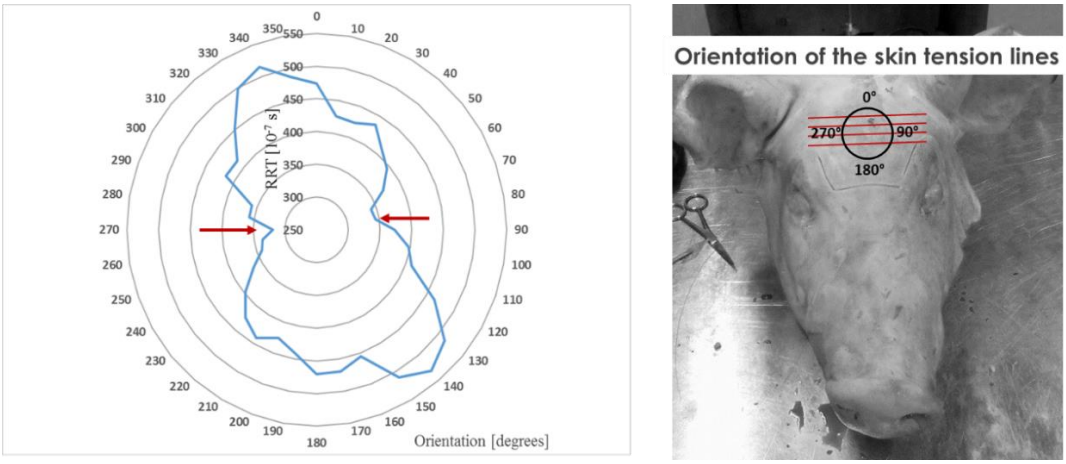

Figure 4: Graph showing the different RRT at different orientations where the arrows represent the minimum RRT and the orientation of the STLs (left). On the right is a picture of the porcine head showing the orientation of the STLs superimposed on the porcine scalp.

3.2 Tensile tests

For each tensile test, a force displacement curve was obtained. The stretch ratio was calculated by dividing the current distance between two horizontal lines drawn on the specimen by the initial distance as shown in Figure 5. The nominal stress was calculated by dividing the force by the undeformed cross-sectional area of the specimen. Assuming incompressibility, the Cauchy stress was then calculated multiplying the nominal stress by the stretch ratio. A number of descriptive parameters were identified and compared (Figure 6): ultimate tensile strength, elastic modulus and failure stretch. Mechanical properties of soft tissues are often dependent on the strain rate of the test and on the orientation of the specimens with respect to the STLs. In order to mechanically characterize scalp tissue for applications in head impact testing, the effect of the strain rate and the orientation were considered.

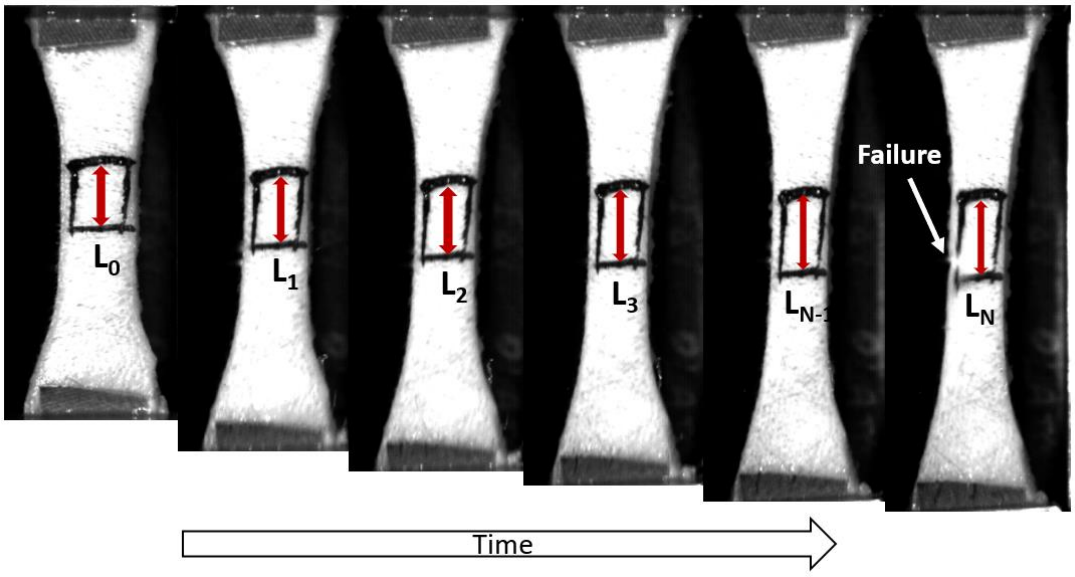

Figure 5: Stretch of the specimen determined as the ratio between the distance of two horizontal lines drawn on the sample at each time step and the initial distance, L_0.

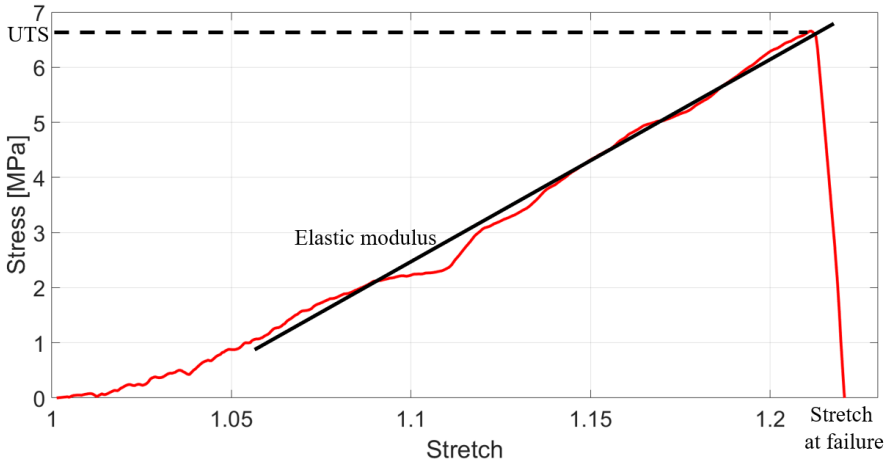

Figure 6: Typical stress-stretch graph for the experimental tests. The UTS is the maximum stress of the specimen before failure. The elastic modulus is defined as the slope of the second linear portion of the curve. The failure stretch is the maximum stretch obtained before failure.

3.2.1 Porcine scalp

Figure 7 shows the averaged tensile tests results performed at different strain rates in the direction of the STLs (in blue) and perpendicular to this direction (in red) on porcine scalp. The increase in strain rate results in an increase in stiffness of the tissue. At low strain rates (0.005 s^{-1}), the scalp appears stiffer when it is loaded parallel to the STLs direction and softer perpendicular to this direction, confirming the anisotropy of this tissue. However, at higher strain rates (15-100 s^{-1}), the level of anisotropy becomes less significant.

Average values of the elastic modulus, UTS and stretch at failure for the porcine scalp at different strain rates and orientations are shown in Figure 8 and reported in Table 1. Results of the multiway ANOVA showed that the strain rate affects (*p-value*<0.05) the UTS (*p-value* = 0.000149), the elastic modulus (*p-value* = $9.16e^{-6}$) and the stretch at failure (*p-value* = $1.15e^{-23}$). The orientation of the sample with respect to the STLs, however, only affects the stretch at failure (*p-value* = 0.0358) but not the UTS (*p-value* = 0.6241) and the elastic modulus (*p-value* = 0.28). One issue commonly encountered when testing biological tissue is the large variation in experimental results. Figure. A. 1, Figure. A. 2, and Figure. A. 3 clearly show the variability at each strain rate for samples loaded in the direction parallel to the STLs (in blue) and perpendicular (in red) by indicating the standard deviation of samples.

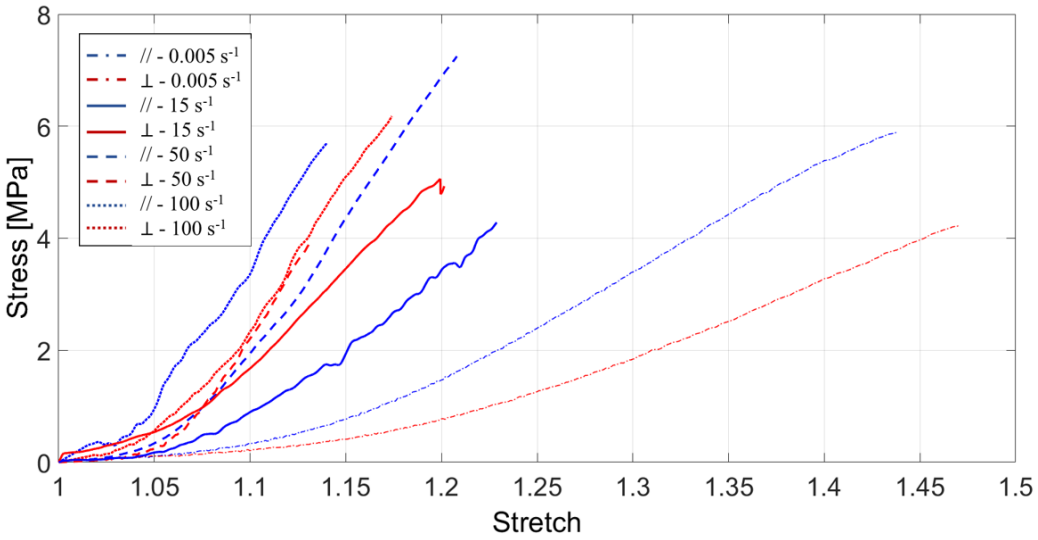

Figure 7: Tensile tests performed on the same porcine scalp on specimens parallel (continuous line) and perpendicular (dashed line) with respect to the STLs. Results are shown in terms of Cauchy stress and stretch.

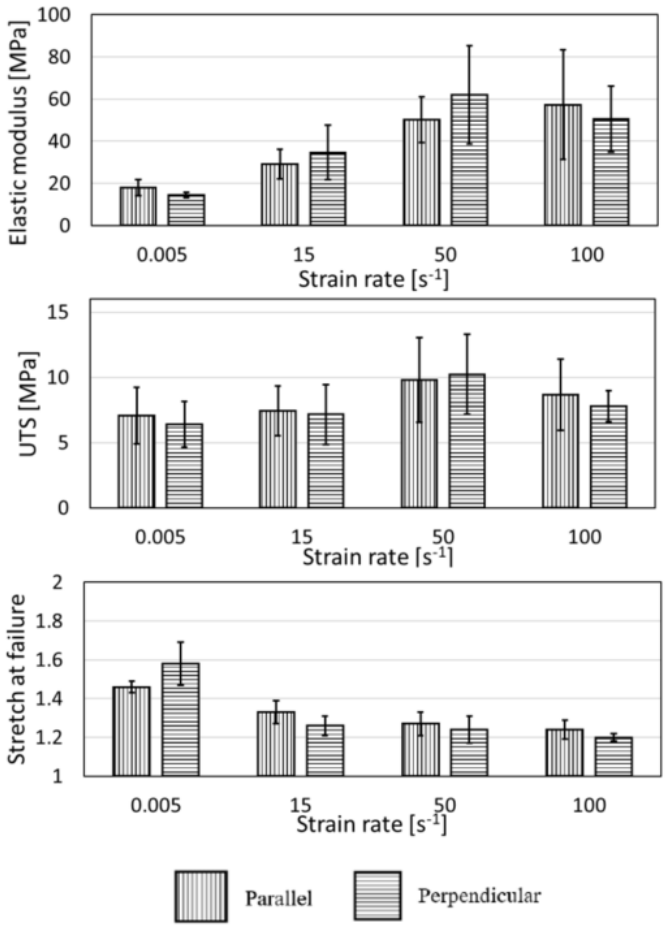

Figure 8: Bar chart of the average elastic modulus, UTS and the stretch at failure of porcine scalp at different strain rates. The error bar represents the standard deviation.

Table 1: Values of the UTS and stretch at failure for porcine specimens parallel and perpendicular with respect to the STLs at different strain rates.

***Strain rate* [s^{-1}]**	***Orientation STLs***	***Elastic Modulus [MPa]***	***UTS* [MPa]**	***Stretch at failure* [-]**
0.005	//	17.94 ±3.78	7.07 ±2.16	1.46 ±0.03
	⊥	14.48 ±1.38	6.39 ±1.75	1.58 ±0.11
15	//	29.01 ±7.01	7.40 ±1.90	1.33 ±0.06
	⊥	34.68 ±12.86	7.16 ±2.29	1.26 ±0.05
50	//	50.20 ±10.90	9.78 ± 3.24	1.27 ±0.06
	⊥	62.11 ±23.28	10.24 ±3.07	1.24 ± 0.07
100	//	57.21 ±26.00	8.68 ±2.72	1.24 ±0.05
	⊥	50.58 ±15.62	7.79 ±1.16	1.20 ±0.02

3.2.2 Human scalp

Figure 9 shows the average results of the human scalp tensile tests performed at different strain rates in the direction of the STLs (in blue) and perpendicular to this direction (in red). Average values of the elastic modulus, UTS and stretch at failure of the human scalp at different strain rates and orientations are shown in Figure 10 and reported in Table 2. Results of a multiway ANOVA showed that the strain rate affects the stretch at failure (*p-value* = 0.0006), but it does not affect the elastic modulus (*p-value* = 0.0111) and the UTS (*p-value* = 0.1526). The orientation of the sample with respect to the STLs does not affect the elastic modulus (*p-value* = 0.1471), the UTS (*p-value* = 0.0397), and the stretch at failure (*p-value* = 0.9202) at dynamic strain rates. The variability for each strain rate and direction is reported in Figure. A. 4, Figure. A. 5, and Figure. A. 6.

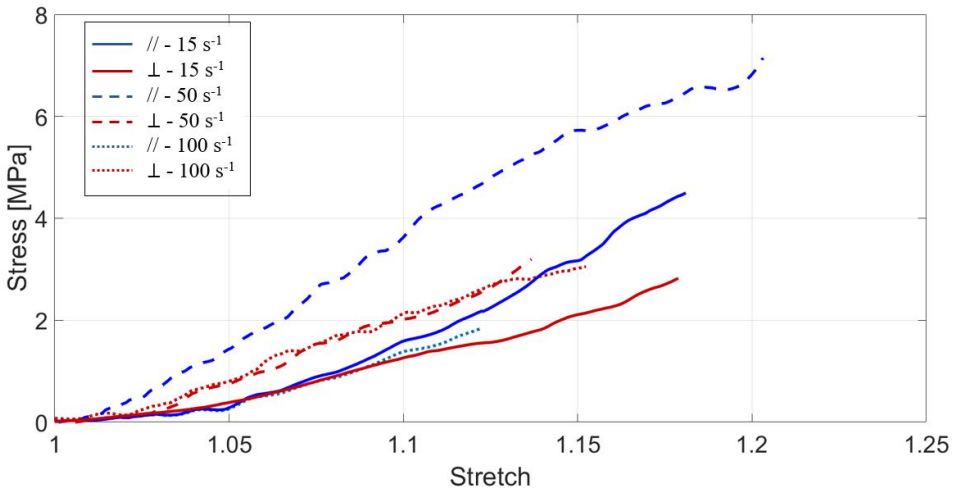

Figure 9: Tensile tests performed on human scalp on specimens parallel (blue line) and perpendicular (red line) with respect to the STLs at different strain rates. Results have been shown in terms of Cauchy stress and stretch.

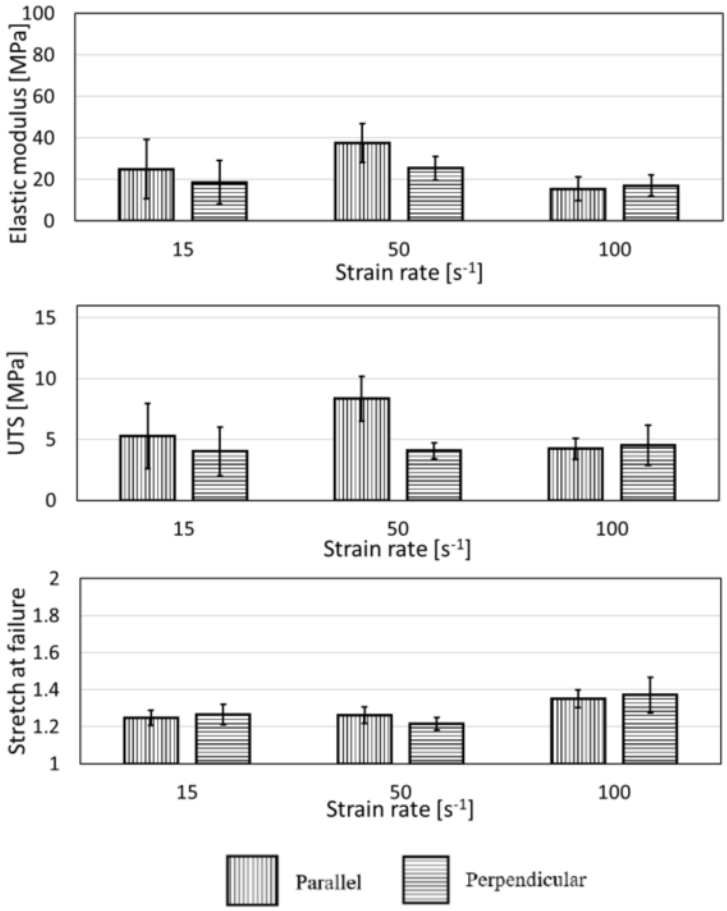

Figure 10: Bar chart of the average elastic modulus, UTS and the stretch at failure of human scalp at different strain rates. The error bar represents the standard deviation.

Table 2: average values of the UTS and stretch at failure for human specimens parallel and perpendicular with respect to the STLs at different strain rates.

***Strain rate* [s^{-1}]**	***Orientation STLs***	***Elastic Modulus [MPa]***	***UTS* [MPa]**	***Stretch at failure* [-]**
15	//	24.96 ±14.35	5.30 ±2.67	1.25 ±0.04
	⊥	18.62 ±10.53	4.01 ±1.99	1.26 ±0.05
50	//	37.56 ±9.30	8.34 ± 1.84	1.26 ±0.04
	⊥	25.36 ±5.69	4.09 ±0.65	1.22 ± 0.03
100	//	15.39 ±5.74	4.23 ±0.85	1.35 ±0.05
	⊥	17.02 ±5.11	4.51 ±1.66	1.37 ±0.09

3.3 Modelling

Due to the anisotropic behaviour of the tissue at low strain rates, the quasi-static data was fit to the GOH model. The average material parameters are given in Table 3. The value of R^2 shows the quality of the fitting. The range of initial guesses (0-$1e^6$ for k1 and 0-$1e^3$) used for the optimization procedure lead to the same set of optimal parameters each time, confirming that the optimization procedure was not sensitive to the initial guess.

Table 3: GOH Model: average material parameters, standard deviation and R^2 of quasi-static porcine scalp tissue

Anisotropic Hyperelastic Model	**μ [MPa]**	**k_1**	**k_2**	***kappa***	***R^2***
GOH	0.57 ±0.16	6.18 ±0.81	3.51e-5 ±1.3e-5	0.05±0.03	0.976

Since the scalp behaves as an isotropic material at high strain rates, three different isotropic hyperelastic models were used to model the high strain rate data. Values of the model parameters were calculated for each orientation and strain rate. Table 4 shows the results of the fitting procedure on porcine scalp while Table 5 shows the results of the fitting for human scalp. The value of R^2 shows good quality of the fitting for each model.

Table 4: Hyperelastic fitting of porcine scalp high strain rate tensile data.

Hyperelastic Model	***Strain rate [s^{-1}]***	**μ [MPa]**	***Stiffening parameter* [-]** ***b (Fung), J_m (Gent), α (Ogden)***	***R^2***
Fung	15	5.21 ±2.47	2.80 ±2.10	0.97
	50	7.66 ±3.85	5.42 ±4.33	0.94
	100	7.50 ±5.01	6.65 ±4.82	0.94
Gent	15	5.58 ±2.39	0.65 ±0.38	0.96
	50	8.40 ±3.62	0.58 ±0.74	0.93
	100	8.20 ±4.82	0.35 ±0.20	0.93
Ogden	15	1.48 ± 1.43	8.10 ± 3.10	0.97
	50	2.30 ±3.53	10.86 ±5.09	0.95
	100	1.47 ±1.63	12.33 ±5.40	0.95

Table 5: Hyperelastic fitting of human scalp high strain rates tensile data.

Hyperelastic Model	***Strain rate [s^{-1}]***	**μ [MPa]**	***Stiffening parameter* [-]** ***b (Fung), J_m (Gent), α (Ogden)***	***R^2***
Fung	15	4.08 ±2.27	3.81 ±1.61	0.98
	50	8.72 ±4.09	3.64 ±5.29	0.97
	100	3.82 ±2.33	2.46 ±3.56	0.97
Gent	15	4.29 ±2.38	0.41 ±0.15	0.98
	50	8.87 ±4.00	0.13 ±2.08	0.97
	100	3.56 ±1.64	0.77 ±0.40	0.95
Ogden	15	0.79 ±0.47	8.99 ±1.88	0.98
	50	3.23 ±2.80	7.95 ±5.57	0.97
	100	1.67 ±2.40	7.84 ±4.29	0.97

Since the multiway ANOVA test described in Section 3.2.2 showed that the strain rate and the orientation of the sample with respect to the STLs does not affect the elastic modulus and the UTS of human scalp tissue, a representative curve for each model can be used to describe the mechanical behaviour of human scalp at strain rates between 15-100 s^{-1}. Averaged human scalp values, among the different strain rates and orientations, of the parameters for the Fung, Gent and Ogden models are reported in Table 6.

Table 6: Parameters of the Fung, Gent and Ogden model describing the representative mechanical behaviour of human scalp tissue between 15-100 s^{-1}.

Hyperelastic model	**μ [MPa]**	***Stiffening parameter* [-]** ***b (Fung), J_m (Gent), α (Ogden)***	**R^2**
Fung	5.53	3.82	0.97
Gent	5.81	0.46	0.96
Ogden	1.48	8.1	0.98

4 Discussion

In order to develop a realistic scalp model, the mechanical characterisation of this tissue must consider different aspects including non-linearity, anisotropy and viscoelasticity. The scalp is generally modelled as a linear elastic material but, due to the importance of the scalp in surgical procedures and head impact biomechanics, there is a need for a thorough and modern mechanical characterisation of this tissue.

Many studies have provided information about the effect of the STLs orientation on the mechanical properties of the skin; some of these base their conclusion on tensile tests [54, 55] and others on in-vivo ultrasonic techniques [47]. As demonstrated by Elastic wave propagation tests and tensile tests performed on samples with different STLs orientations, scalp tissue also presents the same behaviour. Tests using the Reviscometer® device showed that the shock-acoustic wave travels with different speeds around a circular pattern on the scalp. The speed of the generated wave is governed by the density and stiffness and since collagen fibres are stiffer along their axes, this device can identify the orientation of STLs [56]. In this work the Reviscometer® device was only used for the identification of the porcine scalp STLs since this data was already available for human scalp from published literature [48].

Tensile tests performed at different strain rates showed that the scalp mechanical behaviour is highly dependent on strain rate. At higher strain rates (15-100 s^{-1}), scalp tissue is stiffer than at a strain rate of 0.005 s^{-1} and the orientation of the specimen with respect to the STLs (for both human and porcine specimen) does not affect the mechanical properties. This different behaviour might be due to the time required for the fibres' alignment and to the viscoelastic properties of the tissue. Further investigation is necessary to determine the transition between anisotropic and isotropic behaviour. These tests also showed that porcine and human scalp have different mechanical behaviour when subjected to tensile tests. When comparing porcine and human scalp at strain rates between 15-100 s^{-1}, the strain rate was found to affect the elastic modulus, UTS and stretch at failure of porcine scalp, but it was found to affect only the stretch at failure of human scalp. This different behaviour could be in part due to the age of the pigs and cadavers. The porcine scalp tested was harvested from 22 weeks old pigs, while the human scalp was harvested from cadavers 73-89 years old. In the case of the human scalp, the age range was wider, and age is one of the factors known to affect the mechanical properties of the skin [57, 58]. In addition, the effect of the concentration and type of hair follicles between porcine and human scalp might affect the mechanical behaviour of the tissue. The comparison between porcine and human scalp showed a significant difference for the elastic modulus and the UTS, whereas the stretch at failure was not found to be significantly different. The elastic modulus and the UTS of the porcine scalp are almost twice the values of human scalp (Figure 8 and Figure 10). While the use of two dots (or horizontal lines) was sufficient to determine the stretch in the tensile direction, a speckle pattern could provide a more detailed representation of the in-plane deformation.

Figure 11 and Figure 12 show the comparison of the mechanical properties used for modelling scalp tissue in a number of FE head models [18, 19, 59] and the mechanical properties of porcine scalp and human scalp identified in this work, respectively. The comparison shows that a linear elastic material does not represent well the hyperelastic mechanical behaviour of the scalp at all strain rates and orientations.

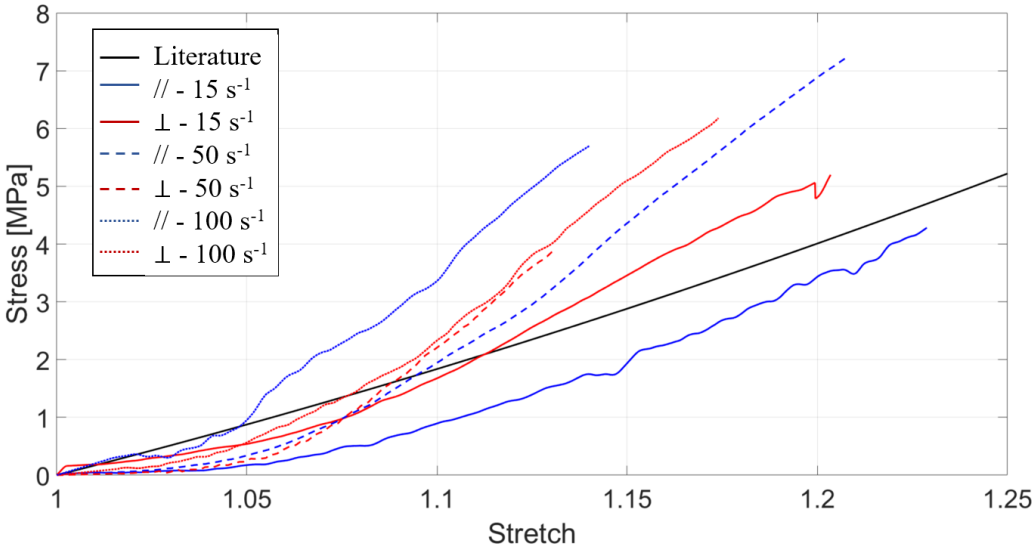

Figure 11: Tensile tests performed at different strain rates on porcine scalp specimens. Specimens were tested in the direction of the collagen fibres (blue line) and in the perpendicular direction (red line). The black line represents the mechanical properties commonly used in literature to represent the scalp [18, 19, 59]. Results are shown in terms of Cauchy stress and stretch.

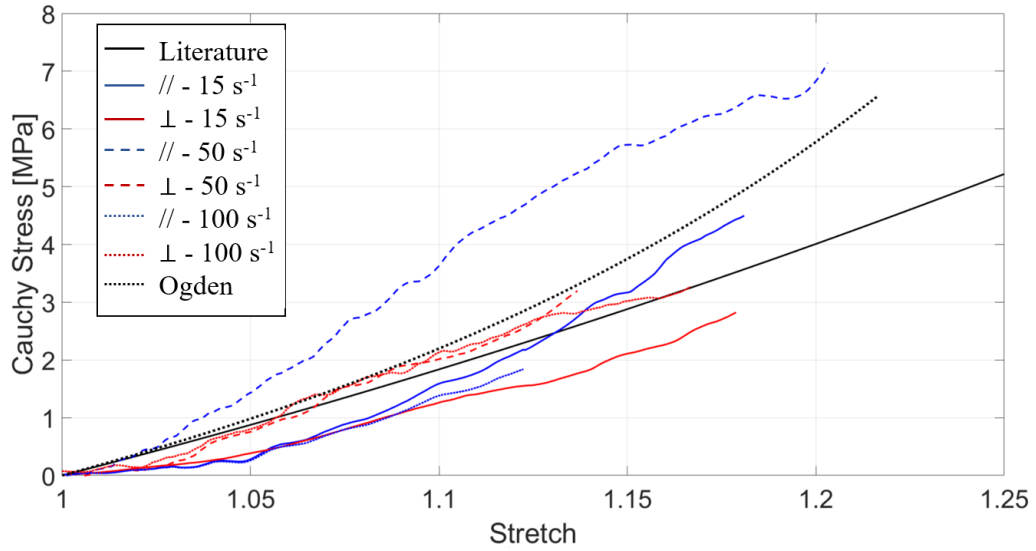

Figure 12: Tensile tests performed at different strain rates on human scalp specimens. Specimens were tested in the direction of the collagen fibres (blue line) and in the perpendicular direction (red line). The continuous black line represents the mechanical properties commonly used in literature to represent the scalp [18, 19, 59]. The dotted black line shows the representative curve for human scalp tissue determined fitting the averaged stress-stretch data with the Ogden model (μ=1.48 MPa and α=8.1). Results are shown in terms of Cauchy stress and stretch.

While skin tissue, in general, has been widely studied, research indicates that the properties of skin depend on body location [54, 60, 61] and function. Mechanical properties of the scalp were found

to be substantially different from the mechanical properties of the skin excised from other parts of the body. Figure 13 shows the comparison between porcine scalp mechanical properties (in red) and porcine skin excised from the belly [62] (dashed black line) while Figure 14 compares tensile tests performed on human scalp (in red) and human skin from the back (dashed black) [63]. In these two cases, scalp tissue presents a softer behaviour than skin from the back and a stiffer behaviour than skin excised from the abdomen.

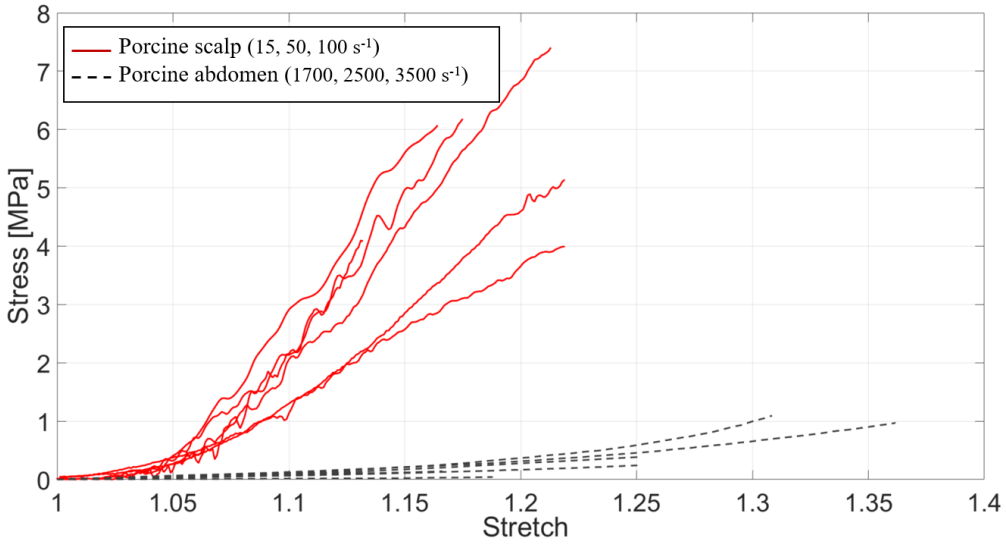

Figure 13: Comparison between tensile tests performed at high speed on porcine scalp (in red) and porcine skin from the abdominal area (dashed black line). Data for porcine skin from the abdominal area was reproduced from Lim et al. [62]. Results are shown in terms of Cauchy stress and stretch.

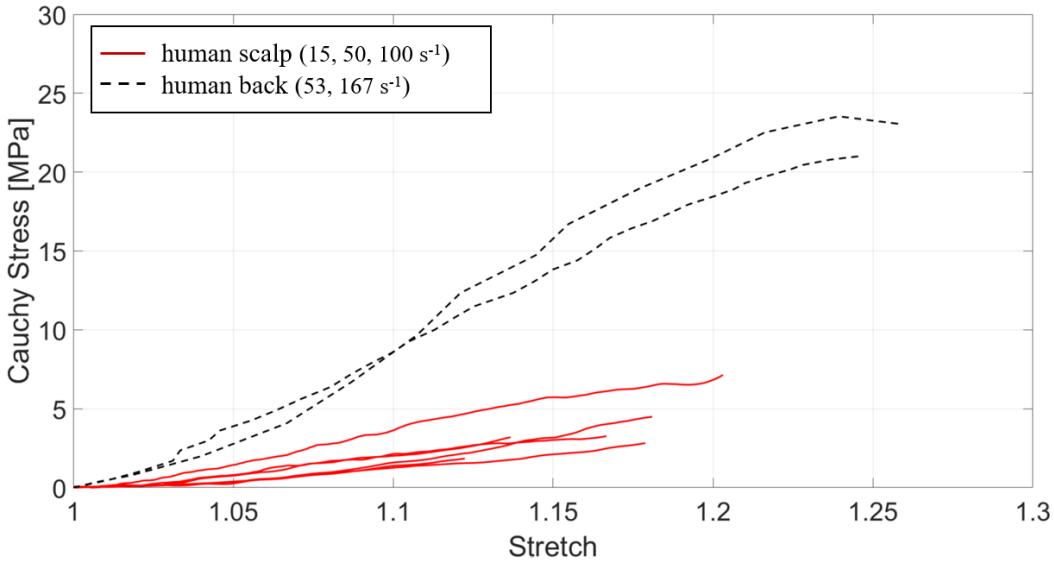

Figure 14: Comparison between tensile tests performed at high speed on human scalp (in red) and human skin from the back (dashed black line). Data for human skin from the back was reproduced from Ottenio et al. [63]. Results are shown in terms of Cauchy stress and stretch.

Since scalp tissue displays different behaviour at quasi-static and high strain rates, the two cases were treated separately. At quasi-static speeds the scalp behaves as an anisotropic material, and

therefore the use of an anisotropic constitutive model was necessary. The experimental data was fit the GOH model using the procedure described by Ní Annaidh et al. [45]. An excellent fit was found for the model with an average R^2 of 0.98. Comparing the results of the fitting on porcine scalp with the ones of human back tissue [54], a significant difference in the values of k_1 and k_2 is noticeable, confirming the importance of the body location when testing the mechanical properties of the skin.

At high strain rates, the scalp behaves as an isotropic material, and therefore a simpler, isotropic hyperelastic model can be used to describe the tissue behaviour. The advantage of this type of model is that they are easy to implement in finite element models. The experimental data from each individual test was fit to the non-linear Fung, Gent, and Ogden models. Excellent fits were found for each model with R^2 ranging from 0.93-0.98 for porcine scalp and 0.93-0.99 for human scalp. The orientation of the sample with respect to the STLs does not affect the mechanical properties at strain rates between 15-100 s^{-1}. The strain rate, instead, was found to affect the mechanical properties of porcine scalp but not those of the human scalp. This behaviour made it possible to identify a representative curve for each one of the three models described in Table 6. Figure 12 shows a representative curve for human scalp tissue using the Ogden model (μ=1.48 MPa and α=8.1).
Limitations of the work include the number, age (only scalp from elderly subjects in this study) and the race (only scalp from Caucasian subject) of the cadavers. In addition, the different size and the storage method of the specimens might influence the mechanical properties, as reported by previous studies [64, 65].

5 Conclusion

This study aimed to characterise mechanical properties of the human and porcine scalp. Tensile tests showed that mechanical behaviour of the scalp differs from the skin from other parts of the body (for instance back and belly). Its response is anisotropic at low strain rates (0.005 s^{-1}) but it can be considered isotropic at high strain rates (15-100 s^{-1}). The mechanical properties of porcine scalp differ from human scalp. In particular, the elastic modulus and the UTS of the porcine scalp were found to be almost twice the values of the human scalp, whereas the stretch at failure was not found to be significantly different. Since the scalp is a complex tissue, the identification of a unique model to describe its behaviour is almost impossible. The choice of the constitutive model must depend on the intended application. For applications in high speed head impact simulations, a non-linear hyperelastic Ogden model represents a good choice. If, for instance, the intended application was to model skin expansion cases, an anisotropic model would be more appropriate.

Acknowledgement

Funding was provided by the European Union's Horizon 2020 research programme under the Marie Sklodowska – Curie grant agreement No. 642662. The authors would like to acknowledge KU Leuven for the use of the testing equipment and Dr Jan Ivens for the help with the ethical approval.

References:

[1] Standring S. Gray's Anatomy International Edition: The Anatomical Basis of Clinical Practice: Elsevier Health Sciences; 2015.
[2] Kumar N, Kumar P, Prasad K, Nayak BS. A histological study on the distribution of dermal collagen and elastic fibres in different regions of the body. International Journal of Medicine and Medical Sciences. 2012;4:171-6.

[3] Seery GE. Surgical anatomy of the scalp. Dermatologic surgery. 2002;28:581-7.
[4] Young RW. Age changes in the thickness of the scalp in white males. Human biology. 1959;31:74-9.
[5] Cormier J, Manoogian S, Bisplinghoff J, Rowson S, Santago AC, McNally C, et al. Biomechanical response of the human face and corresponding biofidelity of the FOCUS headform. SAE International Journal of Passenger Cars-Mechanical Systems. 2010;3:842-59.
[6] Hori H, Moretti G, Rebora A, Crovato F. The thickness of human scalp: normal and bald. Journal of Investigative Dermatology. 1972;58:396-9.
[7] Bauer BS, Johnson PE, Lovato G. Applications of soft tissue expansion in children. Pediatric dermatology. 1986;3:281-90.
[8] Antonyshyn O, Gruss JS, Zuker R, Mackinnon SE. Tissue expansion in head and neck reconstruction. Plastic and reconstructive surgery. 1988;82:58-68.
[9] El-Saadi M, Nasr M. The effect of tissue expansion on skull bones in the paediatric age group from 2 to 7 years. Journal of Plastic, Reconstructive & Aesthetic Surgery. 2008;61:413-8.
[10] Horgan T, Gilchrist M. Influence of FE model variability in predicting brain motion and intracranial pressure changes in head impact simulations. International Journal of Crashworthiness. 2004;9:401-18.
[11] Gurdjian ES. Recent advances in the study of the mechanism of impact injury of the head--a summary. Clinical neurosurgery. 1972;19:1-42.
[12] Hardy CH, Marcal PV. Elastic analysis of a skull: Division of Engineering, Brown University; 1971.
[13] Chan HS. Mathematical model for closed head impact. SAE Technical Paper; 1974.
[14] Khalil TB, Goldsmith W, Sackman J. Impact on a model head-helmet system. International Journal of Mechanical Sciences. 1974;16:609-25.
[15] Gefen A. Studies in Mechanobiology, Tissue Engineering and Biomaterials: Springer; 2009.
[16] Trotta A, Zouzias D, De Bruyne G, Ní Annaidh A. The Importance of the Scalp in Head Impact Kinematics. Annals of biomedical engineering. 2018;46:831-40.
[17] Zhang L, Yang KH, Dwarampudi R, Omori K, Li T, Chang K, et al. Recent advances in brain injury research: a new human head model development and validation. Stapp Car Crash J. 2001;45:369-94.
[18] Belingardi G, Chiandussi G, Gaviglio I. Development and validation of a new finite element model of human head. Proc 19th International Technical Conference of the Enhanced Safety of Vehicle (ESV), Washington, DC2005.
[19] Deck C, Willinger Rm. Improved head injury criteria based on head FE model. International Journal of Crashworthiness. 2008;13:667-78.
[20] Gambarotta L, Massabo R, Morbiducci R, Raposio E, Santi P. In vivo experimental testing and model identification of human scalp skin. Journal of biomechanics. 2005;38:2237-47.
[21] Galford JE, McElhaney JH. A viscoelastic study of scalp, brain, and dura. Journal of biomechanics. 1970;3:211-21.
[22] Jacquemoud C, Bruyere-Garnier K, Coret M. Methodology to determine failure characteristics of planar soft tissues using a dynamic tensile test. Journal of biomechanics. 2007;40:468-75.
[23] Falland-Cheung L, Scholze M, Lozano PF, Ondruschka B, Tong DC, Brunton PA, et al. Mechanical properties of the human scalp in tension. Journal of the mechanical behavior of biomedical materials. 2018;84:188-97.
[24] Ogden R, Deformations N-LE. Dover Publications Inc. Mineola, NY, USA. 1984;984.
[25] Fung Y. Biomechanics: mechanical properties of living tissues. 1993. New York, NY.
[26] Rivlin R. Large elastic deformations of isotropic materials IV. Further developments of the general theory. Phil Trans R Soc Lond A. 1948;241:379-97.
[27] Gent A. A new constitutive relation for rubber. Rubber chemistry and technology. 1996;69:59-61.
[28] Veronda D, Westmann R. Mechanical characterization of skin—finite deformations. Journal of biomechanics. 1970;3:111-24.
[29] Martins P, Natal Jorge R, Ferreira A. A comparative study of several material models for prediction of hyperelastic properties: application to silicone-rubber and soft tissues. Strain. 2006;42:135-47.

[30] Gasser TC, Ogden RW, Holzapfel GA. Hyperelastic modelling of arterial layers with distributed collagen fibre orientations. Journal of the royal society interface. 2006;3:15-35.
[31] Annaidh AN, Ottenio M, Bruyère K, Destrade M, Gilchrist M. Mechanical properties of excised human skin. 6th World Congress of Biomechanics (WCB 2010) August 1-6, 2010 Singapore: Springer; 2010. p. 1000-3.
[32] Horny L, Adamek T, Zitny R. Age-related changes in longitudinal prestress in human abdominal aorta. Archive of Applied Mechanics. 2013;83:875-88.
[33] Rashid B, Destrade M, Gilchrist MD. Mechanical characterization of brain tissue in compression at dynamic strain rates. Journal of the mechanical behavior of biomedical materials. 2012;10:23-38.
[34] Lin DC, Shreiber DI, Dimitriadis EK, Horkay F. Spherical indentation of soft matter beyond the Hertzian regime: numerical and experimental validation of hyperelastic models. Biomechanics and modeling in mechanobiology. 2009;8:345.
[35] Lanir Y, Fung Y. Two-dimensional mechanical properties of rabbit skin—II. Experimental results. Journal of biomechanics. 1974;7:171-82.
[36] Hsu M-C, Kamensky D, Xu F, Kiendl J, Wang C, Wu MC, et al. Dynamic and fluid–structure interaction simulations of bioprosthetic heart valves using parametric design with T-splines and Fung-type material models. Computational Mechanics. 2015;55:1211-25.
[37] Deng S, Tomioka J, Debes J, Fung Y. New experiments on shear modulus of elasticity of arteries. American Journal of Physiology-Heart and Circulatory Physiology. 1994;266:H1-H10.
[38] Tong P, Fung Y-C. The stress-strain relationship for the skin. Journal of biomechanics. 1976;9:649-57.
[39] MacManus DB, Pierrat B, Murphy JG, Gilchrist MD. Region and species dependent mechanical properties of adolescent and young adult brain tissue. Scientific reports. 2017;7:13729.
[40] Lanir Y. Constitutive equations for fibrous connective tissues. Journal of biomechanics. 1983;16:1-12.
[41] Holzapfel GA, Gasser TC, Ogden RW. A new constitutive framework for arterial wall mechanics and a comparative study of material models. Journal of elasticity and the physical science of solids. 2000;61:1-48.
[42] PRAMUDITA JA, SHIMIZU Y, TANABE Y, Masato I, WATANABE R. Tensile Properties of Porcine Skin in Dorsal and Ventral Regions. Journal of the Japanese Society for Experimental Mechanics. 2014;14:s245-s50.
[43] Deroy C, Destrade M, Mc Alinden A, Ní Annaidh A. Non-invasive evaluation of skin tension lines with elastic waves. Skin Research and Technology. 2016.
[44] Courage & Khazaka electronicGmbH K. Information & Oper-ating Instructions for theReviscometerâ RVM 600: Stand-alone and with Software. 2005.
[45] Ní Annaidh A, Bruyere K, Destrade M, Gilchrist MD, Maurini C, Otténio M, et al. Automated estimation of collagen fibre dispersion in the dermis and its contribution to the anisotropic behaviour of skin. Annals of biomedical engineering. 2012;40:1666-78.
[46] Quatresooz P, Hermanns J-F, Hermanns-Le T, Pierard GE, Nizet J-L. Laddering melanotic pattern of Langer's lines in skin of colour. European Journal of Dermatology. 2008;18:575-8.
[47] Liang X, Boppart SA. Biomechanical properties of in vivo human skin from dynamic optical coherence elastography. IEEE Transactions on Biomedical Engineering. 2010;57:953-9.
[48] Langer K. On the anatomy and physiology of the skin. The Imperial Academy of Science, Vienna. British Journal of Plastic Surgery. 1861;17:93-106.
[49] Perogamvros N, Mitropoulos T, Lampeas G. Drop tower adaptation for medium strain rate tensile testing. Experimental Mechanics. 2016;56:419-36.
[50] Yoon S-h, Winters M, Siviour C. High strain-rate tensile characterization of EPDM rubber using non-equilibrium loading and the Virtual Fields Method. Experimental Mechanics. 2016;56:25-35.
[51] Ogden R, Saccomandi G, Sgura I. Fitting hyperelastic models to experimental data. Computational Mechanics. 2004;34:484-502.
[52] Fung Y. Elasticity of soft tissues in simple elongation. American Journal of Physiology--Legacy Content. 1967;213:1532-44.
[53] Ogden R. Large deformation isotropic elasticity—On the correlation of theory and experiment for incompressible rubberlike solids. Rubber chemistry and technology. 1973;46:398-416.

[54] Ní Annaidh A, Bruyère K, Destrade M, Gilchrist MD, Otténio M. Characterization of the anisotropic mechanical properties of excised human skin. Journal of the mechanical behavior of biomedical materials. 2012;5:139-48.
[55] Ridge M, Wright V. The directional effects of skin: A bio-engineering study of skin with particular reference to Langer's lines. Journal of Investigative Dermatology. 1966;46:341-6.
[56] Jor JW, Parker MD, Taberner AJ, Nash MP, Nielsen PM. Computational and experimental characterization of skin mechanics: identifying current challenges and future directions. Wiley Interdisciplinary Reviews: Systems Biology and Medicine. 2013;5:539-56.
[57] Pailler-Mattei C, Bec S, Zahouani H. In vivo measurements of the elastic mechanical properties of human skin by indentation tests. Medical engineering & physics. 2008;30:599-606.
[58] Boyer G, Laquieze L, Le Bot A, Laquieze S, Zahouani H. Dynamic indentation on human skin in vivo: ageing effects. Skin Research and Technology. 2009;15:55-67.
[59] Horgan T, Gilchrist MD. The creation of three-dimensional finite element models for simulating head impact biomechanics. International Journal of Crashworthiness. 2003;8:353-66.
[60] Diridollou S, Black D, Lagarde J, Gall Y, Berson M, Vabre V, et al. Sex-and site-dependent variations in the thickness and mechanical properties of human skin in vivo. International journal of cosmetic science. 2000;22:421-35.
[61] Kalra A, Lowe A, Al-Jumaily A. Mechanical Behaviour of Skin: A Review. J Material Sci Eng. 2016;5:2169-0022.10002.
[62] Lim J, Hong J, Chen WW, Weerasooriya T. Mechanical response of pig skin under dynamic tensile loading. International Journal of Impact Engineering. 2011;38:130-5.
[63] Ottenio M, Tran D, Annaidh AN, Gilchrist MD, Bruyère K. Strain rate and anisotropy effects on the tensile failure characteristics of human skin. Journal of the mechanical behavior of biomedical materials. 2015;41:241-50.
[64] Caro-Bretelle A, Gountsop P, Ienny P, Leger R, Corn S, Bazin I, et al. Effect of sample preservation on stress softening and permanent set of porcine skin. Journal of biomechanics. 2015;48:3135-41.
[65] Marangoni R, Glaser A, Must J, Brody G, Beckwith T, Walker G, et al. Effect of storage and handling techniques on skin tissue properties. Annals of the New York Academy of Sciences. 1966;136:441-53.

Appendix

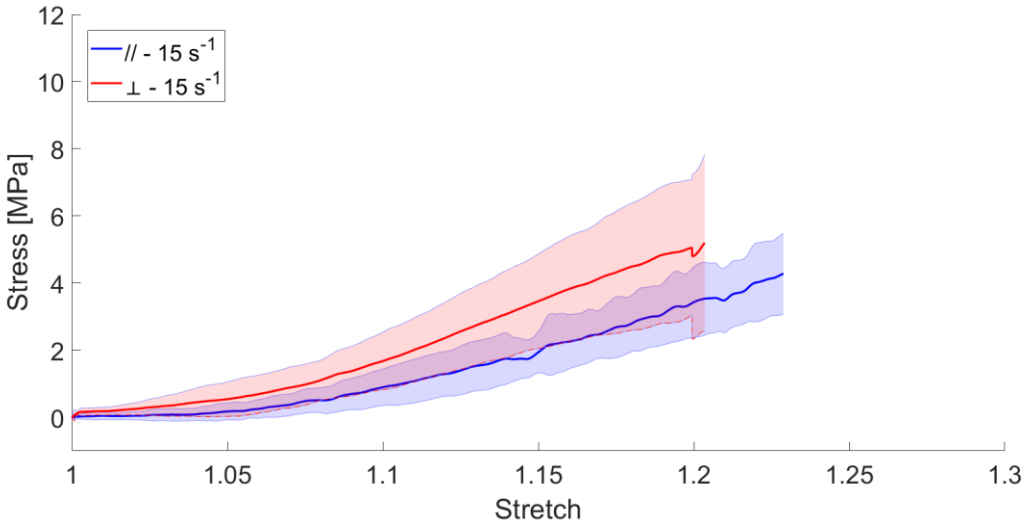

Figure. A. 1: Tensile tests performed on porcine scalp at a strain rate of 15 s^{-1}. The graph shows the average (continuous line) and the standard deviation (shaded area) for specimens parallel (in blue) and perpendicular (in red) with respect to the STLs.

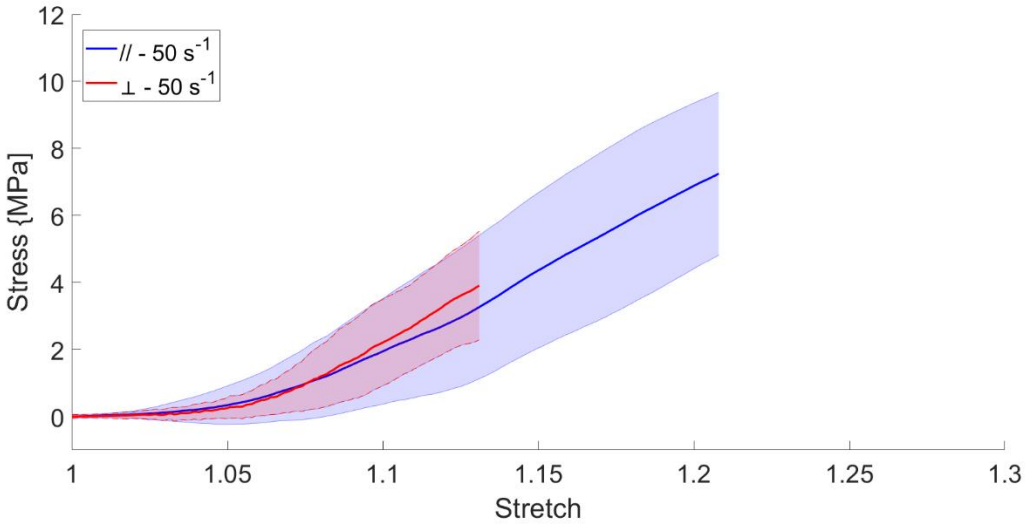

Figure. A. 2: Tensile tests performed on porcine scalp at a strain rate of 50 s^{-1}. The graph shows the average (continuous line) and the standard deviation (shaded area) for specimens parallel (in blue) and perpendicular (in red) with respect to the STLs.

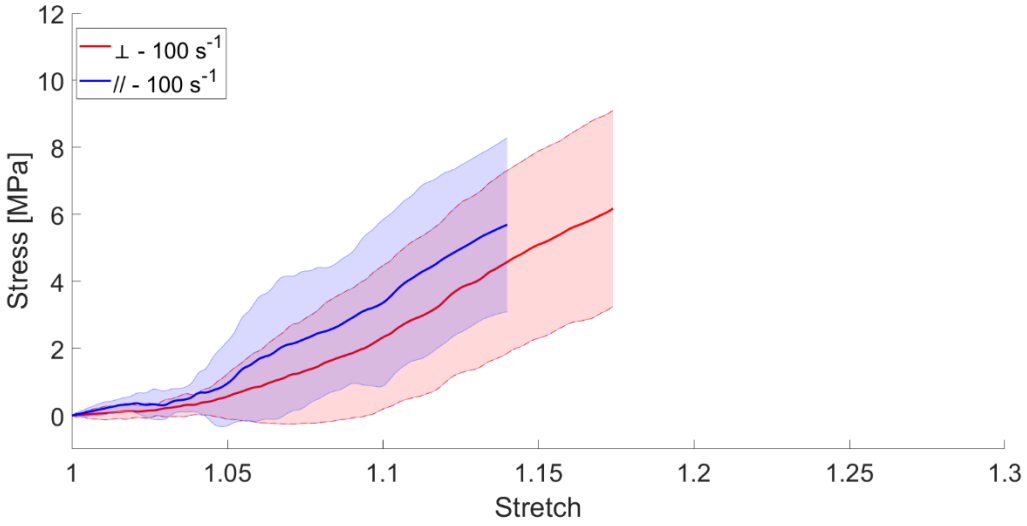

Figure. A. 3: Tensile tests performed on porcine scalp at a strain rate of 100 s^{-1}. The graph shows the average (continuous line) and the standard deviation (shaded area) for specimens parallel (in blue) and perpendicular (in red) with respect to the STLs.

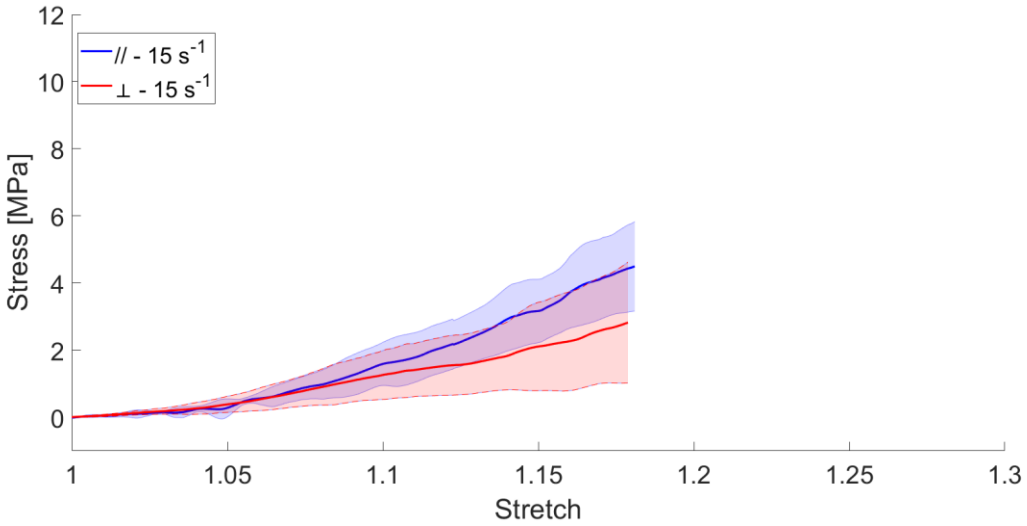

Figure. A. 4: Tensile tests performed on human scalp at a strain rate of 15 s^{-1}. The graph shows the average (continuous line) and the standard deviation (shaded area) for specimens parallel (in blue) and perpendicular (in red) with respect to the STLs.

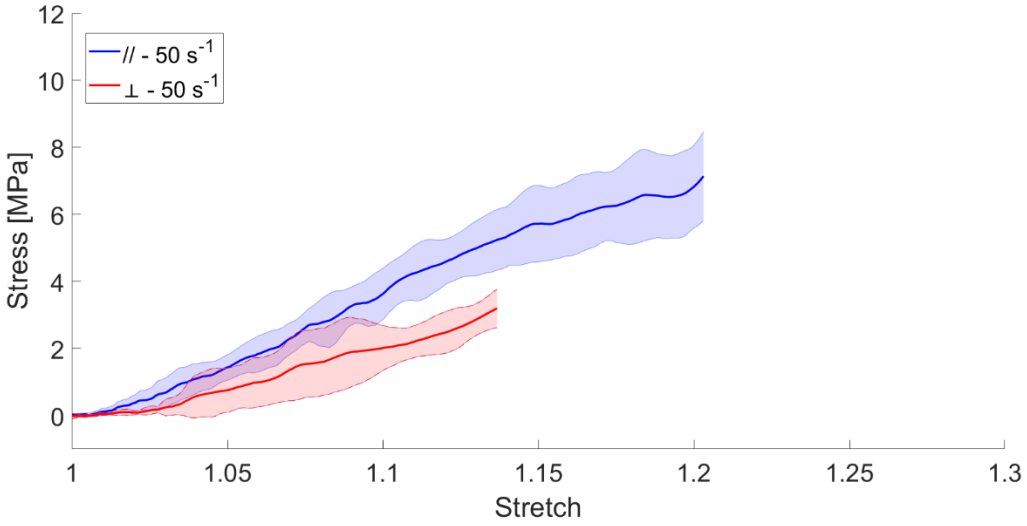

Figure. A. 5: Tensile tests performed on human scalp at a strain rate of 50 s^{-1}. The graph shows the average (continuous line) and the standard deviation (shaded area) for specimens parallel (in blue) and perpendicular (in red) with respect to the STLs.

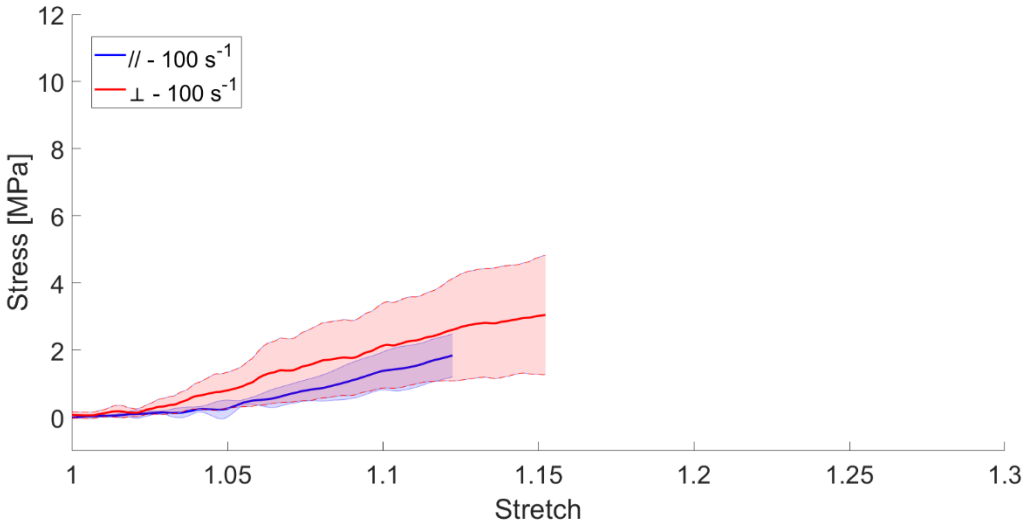

Figure. A. 6: Tensile tests performed on human scalp at a strain rate of 100 s^{-1}. The graph shows the average (continuous line) and the standard deviation (shaded area) for specimens parallel (in blue) and perpendicular (in red) with respect to the STLs.